rf microelectromechanical system device with a lateral field-emission detector*

Kiyotaka Yamashita[a] and Winston Sun
IIS, University of Tokyo, 4-6-1 Komaba, Meguro-Ku, Tokyo 153-8505, Japan

Kuniyuki Kakushima
Tokyo Institute of Technology, 4259 Nagatsuta-cho, Midori-Ku, Yokohama, 226-8503, Japan

Hiroyuki Fujita
IIS, University of Tokyo, 4-6-1 Komaba, Meguro-Ku, Tokyo 153-8505, Japan

Hiroshi Toshiyoshi[b]
IIS, University of Tokyo, 4-6-1 Komaba, Meguro-Ku, Tokyo 153-8505, Japan
and Kanagawa Academy of Science and Technology (KAST), 3-2-1 Sakado, Takatsu-Ku, Kawasaki City, Kanagawa 213-0012, Japan

(Received 12 November 2005; accepted 23 January 2006; published 27 March 2006)

We propose a micromachined device that utilizes the field-emission (FE) phenomenon as a mean to modulate signal for radio-frequency microelectromechanical system applications. In this article, we present the stationary reference (SR) device and the resonator-embedded (RE) device and compare their field-emission performances. The SR device contains no moving part and is used to examine the conditions to excite field emission. The RE device has an embedded microresonator of bandpass filter characteristic. Due to enhanced tip sharpness and closer gap, initial results show that compared to the SR device, the FE current of the RE device has been increased by 192 times under the same anode-cathode potential difference of 240 V and 2×10^{-8} Torr vacuum level. © *2006 American Vacuum Society.* [DOI: 10.1116/1.2177231]

I. INTRODUCTION

Recent development in the field of wireless communication devices and systems has opened up a wide range of electronic applications including cellular phone, wireless local area network (LAN), biomedical diagnosis, security system, and intelligent transportation system (ITS) of automobile. The ultimate target of the wireless technology is to establish the "ubiquitous" computer network by using consumer electronics, which requires further miniaturization of hardware devices that could be produced at lower cost.

Conventional radio-frequency microelectromechanical system (rf-MEMS) mechanical filters[1,2] and recently developed devices[3,4] utilize capacitive coupling for both excitation and detection. However, the capacitance diminishes quickly when the device dimension decreases, which makes signal detection difficult. Besides, direct capacitive coupling often associates with impedance mismatching issues and small fan out.

Recent vacuum microelectronics achievements[5,6] have widened the room for more application opportunities based on the field-emission (FE) effect. Micro- or nanomechanical resonators have the advantages of generally high Q factor, batch fabrication capabilities, and well-established MEMS processes. As device dimensions such as tip radii and anode-cathode gap decreases, field-emission current increases. This work investigates the possibilities of signal detection by integrating the field-emission effect on MEMS device and by comparing the characteristic of the stationary reference (SR) device and that of the resonator-embedded (RE) device; the SR device contains no moving component, whereas a microresonator is integrated to the RE device using the same photolithography step.

II. FIELD EMISSION FOR DETECTING OSCILLATION

The conceptual operation principle for the RE device is illustrated in Fig. 1(a). In between the sharp silicon cathode-anode tips, an electrically biased silicon micromachined resonator is located along the field-emission current path, which is intervened by the resonator as an attempt to modulate the signal that transmits along the FE current. The electrons that pass the fixed screening aperture gates are finally detected by the anode, by which a signal component of a particular frequency is bandpass filtered. The higher the level of vacuum we can achieve, the easier it is for field emission to be excited, and since air damping is reduced, the microresonator can be oscillated at a larger Q factor. Frequency signal picked up by the antenna is preprocessed and fed into the driving electrode for the resonator. The objective of the project is to correlate the information carried by the FE current and the dynamic characteristics of the MEMS resonator. The electrical connections needed to operate the RE device are illustrated in Fig. 1(b), in which the MEMS resonator is implemented as a micromechanical bridge with a movable tip driven by electrostatic coupling. The four tips are arranged in a cross shape that is different from the conceptual

*No proof corrections received from author prior to publication.
[a]Electronic mail: kiyo@iis.u-tokyo.ac.jp
[b]Electronic mail: hiro@iis.u-tokyo.ac.jp

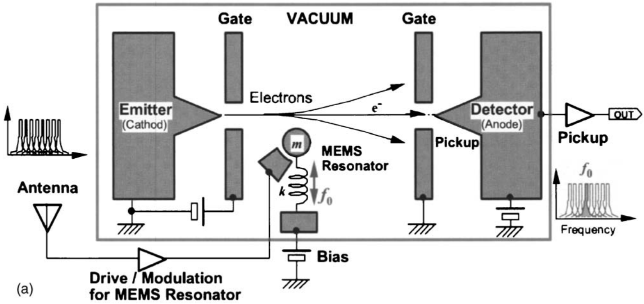

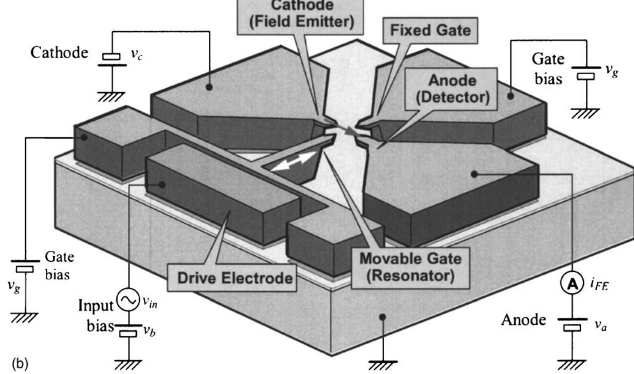

FIG. 1. Conceptual drawing of the proposed resonator-embedded field-emission MEMS device that works as a bandpass filter. (a) Parameters m, f_0, and k are the resonator mass, modulated frequency, and elastic constant of the resonator beam, respectively. (b) Illustration of the electrical wirings for the RE device. v_c, v_a, and v_g are the voltages for the cathode, anode, and the gate, respectively. $v_{\rm in}$ and v_b are the sinusoidal input and constant bias voltages for the resonator, respectively. $i_{\rm FE}$ is the output field-emission current.

drawing shown in Fig. 1(a) such that a small gap could be made by the silicon micromachining technique, as discussed in the following section.

III. FABRICATION

The fabrication process for the RE device is illustrated in Fig. 2. In Fig. 2(a), we began the process with a silicon-on-insulator (SOI) wafer with thicknesses of 10 μm device layer, 2 μm buried oxide (BOX), and 625 μm handle layer. After oxidizing and patterning the oxide mask, the mask pattern is transferred to the device layer by using the deep reactive ion etching (DRIE) process as shown in Fig. 2(b). In Fig. 2(c), the tips were sharpened by the anisotropic wet etching of silicon in a 15 wt % tetramethyl ammonium hydroxide (TMAH) solution at 60 °C. Under the protection of the oxide mask, TMAH anisotropic etching from the sides causes the beam cross sections to become trapezoidal or even triangular. Once TMAH etching is adequate to separate these narrow connecting beams, the oxide mask can be remove in a buffered HF (BHF) solution. More timed TMAH etching to further sharpen the tips might be necessary.

As leakage current is related to the surface conditions at the interface between the BOX layer and the handle layer, the timed partial BOX etching[7] in Fig. 2(d) becomes a critical step. At the current stage, the exact mechanism of how leakage current is related to the residual stress at the interface

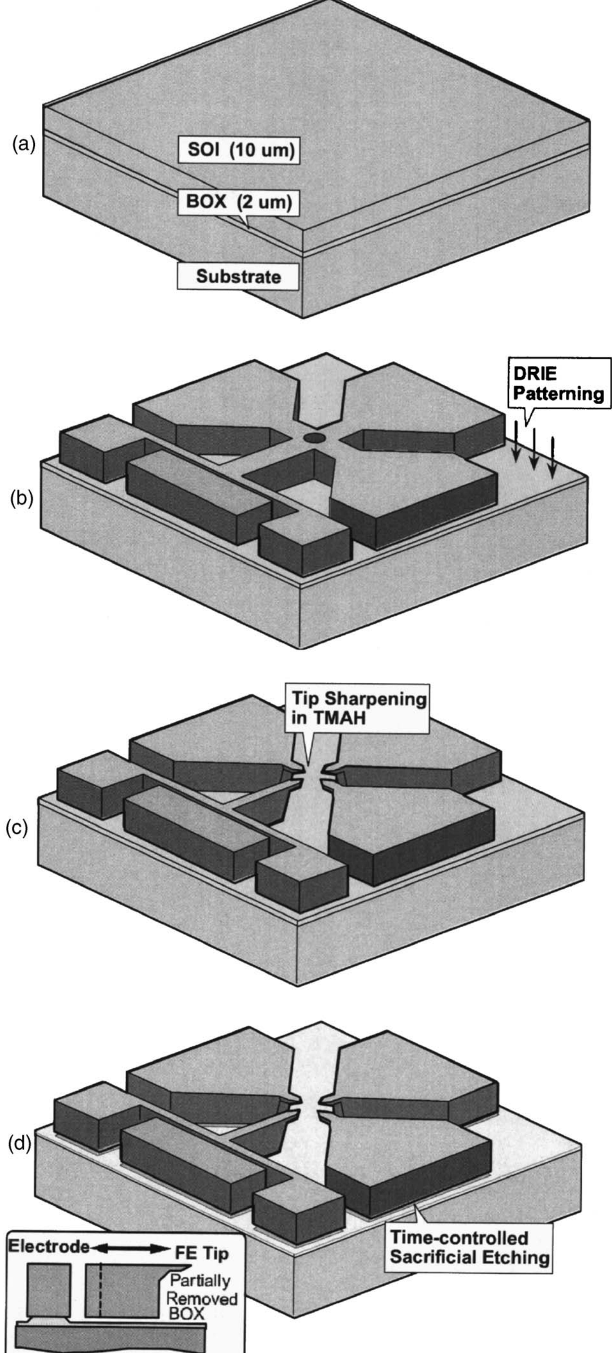

FIG. 2. Fabrication process illustrates how the sharp anode-cathode tips of the RE device are formed. The same process can also be used on the SR device except that the vapor-HF etching is optional. (a) The process begins with transferring the mask pattern to the front side of an oxidized SOI wafer. (b) With the protection of an oxide mask, TMAH etching shapes the precursor tips. (c) Oxide mask removal and further TMAH etch separate and sharpen the tips. (d) Partial vapor-HF etch appears to help reduce leakage current. Exact reason for such behavior is not fully understood.

layer and how it can be confidently avoided remain unclear to us. For the RE device that contains a resonator, we used vapor-phase HF etching to prevent movable components from sticking to the substrate.[8] The etching time must be adequate to sacrificially release the MEMS resonator but not too long to completely remove the exposed BOX layer. The

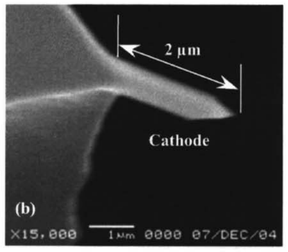

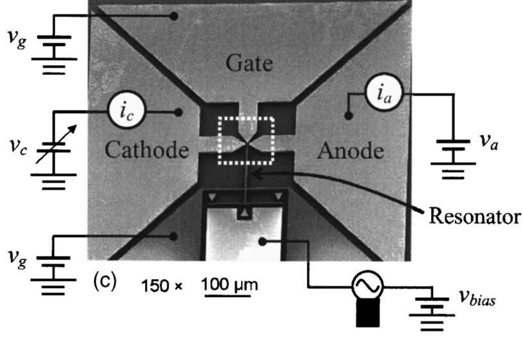

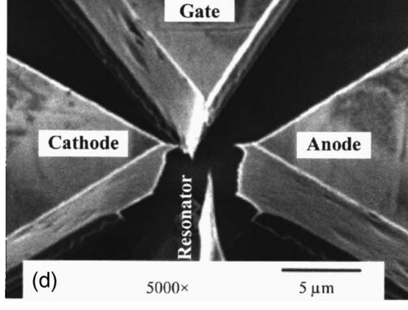

FIG. 3. (a) SEM picture of the SR device showing that the anode-cathode gap is about 5 μm. (b) A close-up at the cathode tips. (c) Electrical connection schematics overlaying with the SEM picture of the whole RE device. In our experiment, the gate voltages are equipotential with the anode voltage. (d) SEM picture focused on the TMAH-processed tips of the RE integrated device. Anode-cathode gap is reduced to about 3 μm.

fabrication procedures are the same for the SR device except that vapor-HF etching is not needed as it contains no moving part. The overall fabrication process contains only one photolithography step, one deep RIE step, and several chemical etching steps. The present process for making sharp tips is more straightforward than the tip sharpening by stress-induced thermal oxidation,[9] and it could be completed by shorter processing time. The chip was then placed under a microscope on a probe station. The microactuators were mechanically displaced by probes to determine if the resonators were fully released and whether further etching would be needed. Once successful release was ensured, the chip was then wire bonded to a chip holder. After connecting a device to an ac power supply, mechanical oscillation at the tip was to be observed.

Scanning electron microscope (SEM) pictures of the SR device and a close-up view at one of its tips are shown in Figs. 3(a) and 3(b), respectively. The anode-cathode gap is observed to be about 5 μm. Figure 3(c) shows the RE device with the corresponding electrical connections. A close-up view at its tips is shown in Fig. 3(d). Fabrication improvements on both the tip sharpness as well as the gap distance between the cathode and the anode tips of this device were achieved. Due to the tailored etching timing, the anode-cathode gap is observed to be reduced to about 3 μm.

IV. EXPERIMENT

The experimental setup includes a semiconductor parameter analyzer (SPA, Agilent E5263A) and the vacuum chamber that provides the 2×10^{-8} Torr (2.7×10^{-6} Pa) vacuum environment. The current flow through the anode channel i_a and cathode channel i_c as shown in Fig. 3(c) can be measured simultaneously by the SPA. A multichannel electrical interface is used to provide electrical feedthrough to the chipset from outside the vacuum chamber. In our experiment, one output channel of the SPA provides a constant positive anode voltage ν_a, which is equipotential to the gate voltages ν_g, and the other output channel sweeps a negative cathode voltage ν_c, while the SPA simultaneously captures the electrical current variation along the circuit in the nanoampere range. The general purpose interface bus (GPIB) input/output (I/O) interface of the SPA is connected via a GPIB-universal serial bus (USB) conversion module to a personal computer (PC) installed with the LABVIEW® software. An interface program is written for control and data acquisition.

V. RESULTS AND DISCUSSION

The field-emission phenomenon can be mathematically described by the governing Fowler-Nordheim[5,10] (FN) equation shown in (1). It expresses the FE current density J as a function of the external electric field F and the material work function ϕ (~4.5 eV for bare silicon),

$$J = 1.54\times10^{-6}\frac{F^2}{1.1\phi}\exp\left(-6.83\times10^{7}\frac{\phi^{3/2}}{F}\left(0.95 - \left(\frac{3.79\times10^{-4}\sqrt{F}}{\phi}\right)^{2}\right)\right). \quad (1)$$

In (1), the units of the FE current density J and external electric field F are A cm^{-2} and V cm^{-1}, respectively. The FE current i_{FE} can be expressed in terms of J and the effective FE tip area α as shown in (2),

$$i_{\mathrm{FE}} = \alpha J. \quad (2)$$

The relation between F and the electric field coefficient β and the anode-cathode potential difference ν_{ac} is shown in (3),

$$F = \beta|\nu_a - \nu_c| = \beta\nu_{\mathrm{ac}}. \quad (3)$$

For the SR device, the values of α and β are estimated to be 8.9×10^{-14} cm^2 and 6.4×10^{5} cm^{-1}, respectively. By combining and rearranging (1)–(3), the field-emission current i_{FE} can be written in terms of the anode-cathode potential difference ν_{ac}, effective tip area α, electric field coefficient β, and work function ϕ as shown in (4),

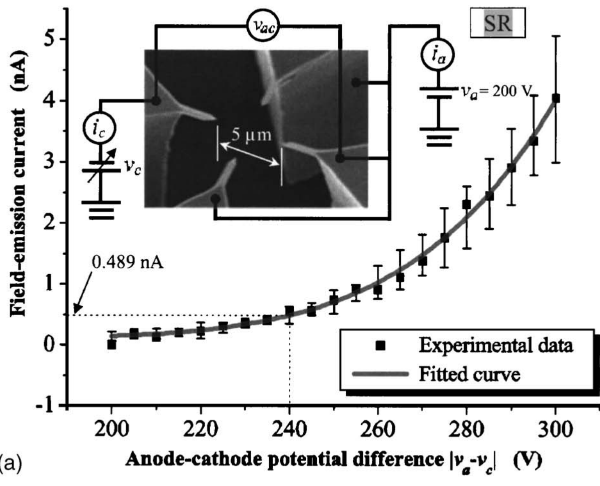

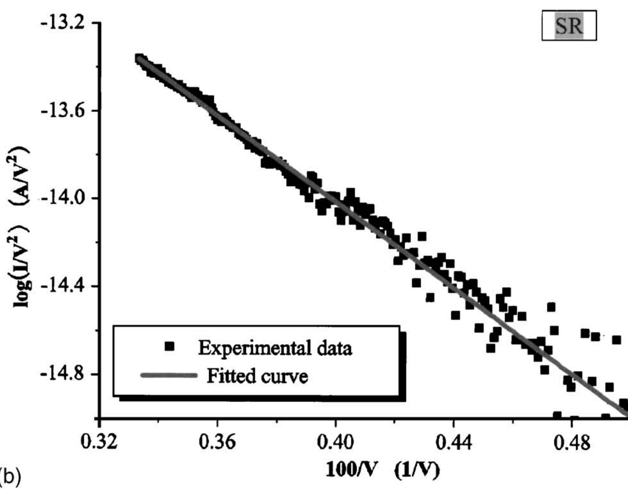

FIG. 4. (a) *I-V* characteristic curve of the SR device. Experimental data agree well with theory. Each data point is averaged from five measurements with error bars of one standard deviation. Anode voltage ν_a is fixed at 200 V. Cathode voltage ν_c varies from 0 to 100 V. At a 240 V anode-cathode potential difference, FE current is measured to be about 0.489 nA. Current flows through the cathode channel i_c and the anode channel i_a are equal with opposite signs, which indicates that the leakage current flow through the substrate is negligible. (b) Corresponding FN plot. A straight line curve fitting clearly indicates the occurrence of the FE effect.

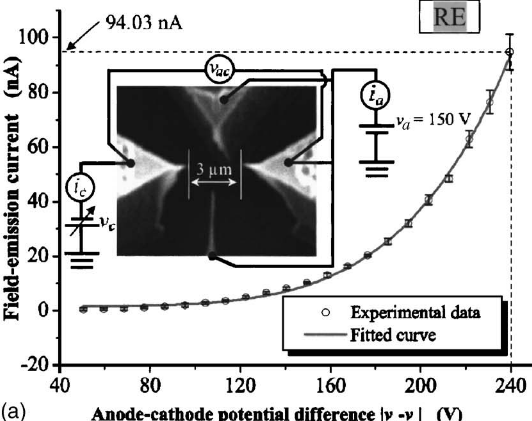

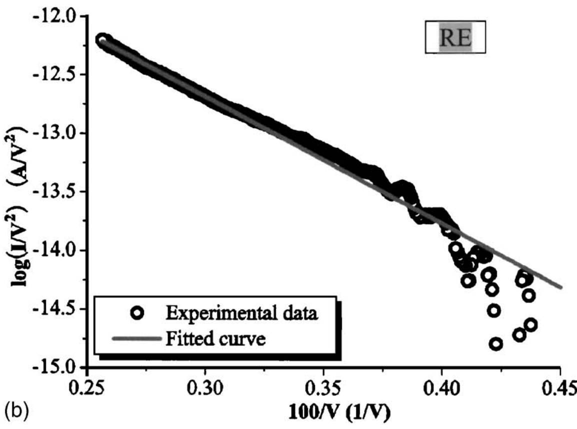

FIG. 5. (a) *I-V* characteristic curve of the RE device. Each data point is averaged from five measurements with error bars of one standard deviation. Slightly varied TMAH etching time produces closer gap of 3 μm and sharper tips which result in larger FE current. Anode voltage ν_a is fixed at 150 V. Cathode voltage ν_c varies from 0 to −90 V. At a 240 V anode-cathode potential difference, the FE current is measured to be about 94.03 nA, which is a 192 times improvement with respect to the SR device. (b) The experimental data in the corresponding FN plot can also be fitted with a straight line.

$$i_{\mathrm{FE}} = \left(1.42 \times 10^{-6} \frac{\alpha\beta^2}{\phi} \exp\left(\frac{10.4}{\sqrt{\phi}} - \frac{6.44 \times 10^7 \phi^{3/2}}{\beta \nu_{\mathrm{ac}}}\right)\right) \nu_{\mathrm{ac}}^2. \tag{4}$$

The experimentally acquired FE current data can now be fitted with (4). As shown in the *I-V* curve of the SR device with a 5 μm anode-cathode gap [see Fig. 3(a)] in Fig. 4(a), the experimental data agrees well with the theory. At a bias voltage of 300 V (anode and cathode are at +200 and −100 V, respectively, and gate voltages are equipotential with anode), the FE current was measured to be 4 nA. The magnitudes of the current flow through the cathode channel i_c and the anode channel i_a are equal but with opposite signs. This indicates that the leakage current through the substrate was negligible. A corresponding FN plot is shown in Fig. 4(b). A straight line fit clearly indicates that the current acquired was excited by the field-emission effect.

The FE effect was also achieved in the RE device. After tailoring the device design and the fabrication conditions, the anode-cathode gap of the RE device was reduced to 3 μm, and the FE current was measured to be over 90 nA at a bias voltage of 240 V as shown in Fig. 5(a). The values of α and β were estimated to be 1.1×10^{-13} cm^2 and 5.8×10^5 cm^{-1}, respectively. A corresponding FN plot is shown in Fig. 5(b). For comparison purpose, at a 240 V anode-cathode voltage, the FE currents of the SR and the RE devices are estimated from their corresponding fitted curves to be 0.489 and 94.03 nA, respectively. A 2 μm gap reduction and sharpness enhancement give a 192 times FE current improvement. We believe that the FE performance could be further improved by coating the emitter tips with materials of lower work functions, such as molybdenum (Mo) or carbon nanotube (CNT).

VI. CONCLUSION AND OUTLOOK

The stationary reference (SR) device and the resonator-embedded (RE) device for MEMS rf bandpass filter have

TABLE I. Comparison between the SR device and the RE device.

	Stationary Reference (SR) device	Resonator Embedded (RE) device
SEM Image		
Gap between tips	5 μm	3 μm
Estimated tip diameter	100 nm	50 nm
FE current at 240 V anode cathode potential difference	0.49 nA	94 nA

been fabricated using simple one-mask process based on the silicon micromachining technology. The field-emission (FE) effect was clearly observed on both devices. A comparison between the SR device and the RE device is shown in Table I. Thanks to a refined fabrication process, the FE current of the RE device is 192 times higher than that of the SR device. However, we noticed drifting of the FE current as experiment duration prolonged. Possible cause is that the bare silicon tips are, in fact, slowly being damaged. Also, taking the chip out from the vacuum chamber oxidizes the tips rapidly. Leakage current dominates and no FE effect can be observed when the chip is put back into the vacuum chamber and reoperated at the same vacuum level. Possible solution is to metallize the tips with materials of lower work function to increase the FE current, decrease the threshold voltage, and delay the oxidation.

The RE device with integrated MEMS oscillator has also been successfully fabricated and released by vapor HF. Oscillation can be observed by inputting an ac signal. The next step is to design a device with increased resonance frequency and to demonstrate modulation capabilities.

We are also interested to look into the following issues in order to make the operation of the device portable. First, both the threshold voltage and operation voltage must be further lowered such that high-voltage power supply is not needed. Second, the effect of an oxygen-free working environment on the FE current will be studied. We will investigate how to effectively and reasonably package the device such that expensive high vacuum packaging is not needed.

ACKNOWLEDGMENTS

This research is partially supported by the 21st Century COE (center of excellence) program in Electrical Engineering and Electronics, University of Tokyo. Part of the work was supported by the Grant-in-Aid for Scientific Research (S) provided by the Japanese Society for Promotion of Science (JSPS). Photolithography masks were fabricated using EB lithography apparatus of VLSI Design and Education Center (VDEC) at the University of Tokyo.

[1]L. Lin, R. T. Howe, and A. P. Pisano, J. Microelectromech. Syst. **7**, 286 (1998).
[2]K. Wang and C. T.-C. Nguyen, J. Microelectromech. Syst. **8**, 534 (1999).
[3]M. U. Demirci and C. T.-C. Nguyen, *Proceedings of the 18th IEEE International Conference on Microelectromechanical Systems 2005, Miami, FL, 30 January–3 February 2005* (IEEE, New York, 2005), p. 207.
[4]Y. Xie, S. S. Li, Y. W. Lin, Z. Ren, and C. T.-C. Nguyen, *Proceedings of the 18th IEEE International Conference on Microelectromechanical Systems 2005 Miami, PL, 30 January–3 February 2005* (IEEE, New York, 2005), p. 219.
[5]D. Temple, Mater. Sci. Eng., R. **24**, 185 (1999).
[6]Y. Takiguchi, *et al.* IEICE Trans. Electron. **E85-C**, 1916 (2002).
[7]N. Nozawa, K. Kakushima, G. Hashiguchi, and H. Fujita, Proceedings of the third Workshop on Physical Chemistry of Wet Etching of Silicon, Nara, Japan, 4–6 June 2002 (unpublished), pp. 52–53.
[8]Y. Fukuta, H. Fujita, and H. Toshiyoshi, Jpn. J. Appl. Phys., Part 1 **42**, 3690 (2003).
[9]H. Toshiyoshi, M. Goto, M. Mita, H. Fujita, D. Kobayashi, G. Hashiguchi, J. Endo, and Y. Wada, Jpn. J. Appl. Phys., Part 1 **38**, 7185 (1999).
[10]R. H. Fowler and D. L. Nordheim, Proc. R. Soc. London, Ser. A **19**, 173 (1928).